Pure & Appl. Chem., Vol. 65, No. 11, pp. 2335–2342, 1993.
Printed in Great Britain.

Investigations of dioxygen reactivity with synthetic models of the metalloproteins hemocyanin and cytochrome *c* oxidase

Stephen Fox, Alaganandan Nanthakumar, Ning Wei, N. Narasimha Murthy and Kenneth D. Karlin*

Department of Chemistry, Charles and 34th Streets, The Johns Hopkins University, Baltimore, Maryland 21218, U. S. A.

Abstract
Synthetic, chemical, and low-temperature stopped-flow kinetic studies in EtCN indicate initial formation of the 1:1 O_2 adduct $[(TMPA)Cu(O_2)]^+$ (**4**), and subsequent formation of the 2:1 O_2 adduct $[\{(TMPA)Cu\}_2(O_2)]^{2+}$ (**2**) from $[(TMPA)Cu(RCN)]^+$ (**1**) and O_2; vacuum-cycling experiments demonstrate reversible binding of O_2. An X-ray structural study of **2** revealed a *trans*-μ-1, 2 configuration for the O_2^{2-} ligand; thus, the reactivity of **1** with O_2 models the function of hemocyanin. Reaction of **1** with $(F_8\text{-TPP})Fe(II)pip_2$ (**5**) and O_2, yielded the structurally characterized μ-oxo $[(F_8\text{-TPP})Fe(III)\text{-}O\text{-}Cu(II)(TMPA)]^+$ (**6**) species, which was protonated to yield the μ-hydroxo bridged analogue $[(F_8\text{-TPP})Fe\text{-}(OH)\text{-}Cu(TMPA)]^{2+}$ (**9**); these complexes may model intermediates in the O_2 reduction cycle, and/or the "resting-state", of cytochrome *c* oxidase.

INTRODUCTION

Nature has selected certain copper (Cu)-containing proteins, not to mention other metalloproteins, to carry out a variety of processes involving dioxygen (O_2) (ref. 1). As shown in Table 1, these include O_2 transport, as performed by hemocyanin; oxygen-atom insertion into C-H bonds, as performed by monooxygenases; the reduction of O_2 to H_2O_2 or H_2O in respiration, as performed by oxidases; and the proposed destruction of the toxic superoxide ion (O_2^-) by the aptly named superoxide dismutase. We, and others, (refs. 2, 3) have endeavored to understand the structure and function of these classes of proteins through the syntheses of active-site analogs -- molecules which model the essential metal-ligand coordination of the protein active-site -- and, subsequently, their reactivity with O_2. Although our research group has discovered some remarkable monooxygenase-type chemistry, (ref. 2, 4) this article will focus on some of our principal findings concerning the reversible binding of O_2, which is pertinent to O_2 transport, as well as our synthesis and study of an oxo-bridged binuclear porphyrin-iron-copper complex as a model for the resting-state of cytochrome *c* oxidase (CcO).

TABLE 1. Main classes of copper proteins involved in O_2 processing.

PROTEIN	SOURCE	BIOLOGICAL FUNCTION
Oxygen Carrier		
Hemocyanin (Hc)	Molluscs and Arthropods	O_2-transport
Copper Monoxygenases		
Tyrosinase (Tyr)	Fungal, Mammal	Tyrosine oxidation
Dopamine β-hydroxylase (DβH)	Adrenal, Brain	Dopamine → Norepinephrine
Peptidylglycine α-Amidating Monooxygenase (PAM)	Pituitary, Heart	Oxidative N-dealkylation
Phenylalanine Hydroxylase (PAH)	Chromobacterium violaceum	Phenylalanine → Tyrosine
Methane Monooxygenase (MMO)	Methanogenic bacteria	Methane → Methanol
Copper Oxidases		
Ascorbate Oxidase (AO)	Plants	Oxidation of L-Ascorbate
Cytochrome *c* Oxidase (CcO)	Mitochondria	Terminal oxidase (Proton pump)
Other		
Superoxide Dismutase (SOD)	Red blood cells, animals	O_2^- detoxification

O_2 CHEMISTRY OF CU(I) COMPLEXES CONTAINING TRIPODAL LIGANDS

A recurring feature in protein Cu-O_2 chemistry is the utilization of histidine, that is, imidazolyl ligation. A now classic example is that of the deoxy-oxy hemocyanin couple, whose structure and function are shown in Fig. 1 (ref. 5, 6).

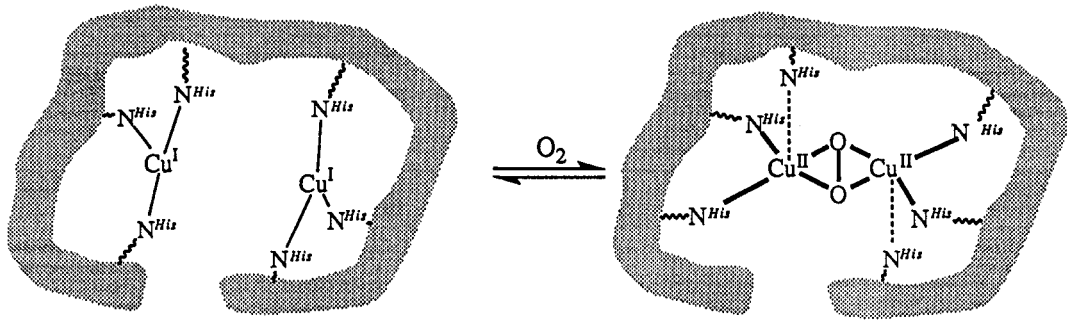

***deoxy*-Hemocyanin** colorless

Panulirus interruptus (spiny lobster):
low pH form: Cu...Cu = ~ 3.6 Å (X-ray)
distorted 3-coordination

Limulus II (horseshoe crab):
Cu...Cu = 4.6 Å
Trigonal-planar Cu(I), Cu-N ~ 2.0 Å

***oxy*-Hemocyanin** blue

Limulus II (horseshow crab):
Cu...Cu = 3.6 Å (X-ray)

ν(O-O) ~ 750 cm^{-1} (resonance Raman)
Tetragonal Cu(II) (Spectroscopy)
λ_{max} = 345 (ε~20,000), 485 (CD), 570 nm (1,000)
Diamagnetic (-2 J > 600 cm^{-1})

Fig. 1. The deoxy-oxyhemocyanin couple: its reversible O_2 binding and other properties.

In order to model the neutral, aromatic, nitrogenous imidazolyl character, some of our studies have utilized the synthetically accessible tripodal, chelating pyridyl ligands TMPA (ref. 7), TEPA, and derivatives thereof (Fig. 2). Investigations involving reactions of O_2 with mononuclear $[LCu]^+$ complexes, where L = TMPA = tris[(2-pyridyl)methyl]amine (Fig. 2), have resulted in significant advances in our understanding of Cu_2O_2 complexes. The first X-ray structurally characterized Cu_2O_2 species, the *trans*-μ-1,2-peroxo $[\{(TMPA)Cu\}_2(O_2)]^{2+}$ (2), was formed from the reaction of $[(TMPA)Cu(RCN)]^+$ (1) with O_2 at -80 °C in EtCN or CH_2Cl_2 (Cu:O_2 = 2:1, manometry) (Fig. 3). Under similar conditions, $[(TEPA)Cu]^+$ (3), where TEPA has an extra CH_2 group between the 2-pyridyl and tertiary amine nitrogen compared to TMPA, does not react with O_2. Presumably, the more positive redox potential of $[(TEPA)Cu]^+$ vs. $[(TMPA)Cu(RCN)]^+$ (Fig. 2) results in this inertness towards O_2. In any event, we note that synthetically modifying the skeleton of our chelating ligand can induce drastic changes in the reactivity of its complexes with O_2.

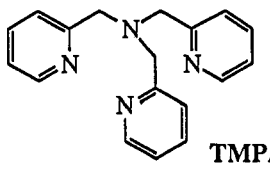

TMPA

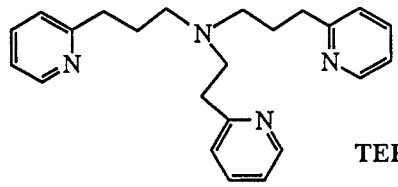

TEPA

$[Cu(TMPA)(RCN)]^+$ (1)
$E_{1/2}$ = -0.01 V
vs Ag/AgCl in C_2H_5CN

$[Cu(TEPA)]^+$ (3)
$E_{1/2}$ = 0.44 V
vs Ag/AgCl in C_2H_5CN

Fig. 2. Comparison of the chelating tripodal ligands TMPA and TEPA.

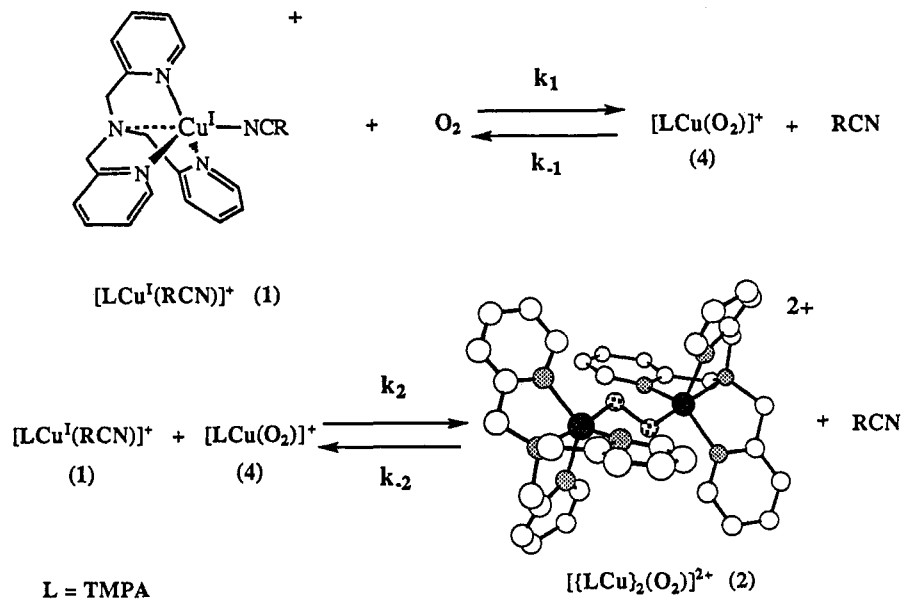

Fig. 3. Reversible O_2 binding to synthetic Cu(I) complex: the proposed reactivity scheme.

Physical Properties of *trans*-μ-1,2-(O_2^{2-}) $[\{(TMPA)Cu\}_2(O_2)]^{2+}$ (2) (ref. 7)

At low temperature (-90 °C), O_2 binds to complex **1** to form an intense purple solution with strong absorptions at λ_{max} = 440 nm (ε = 2000 $M^{-1}cm^{-1}$), 525 nm (11500), and 590 nm (sh, 7600) -- all assigned to O_2^{2-} to Cu^{2+} charge-transfer transitions. In addition, there is a d-d band at 1035 nm (180). Although O_2 binds strongly to complex **1** at low temperature, it can be removed reversibly by vacuum cycling experiments (Fig. 4), i.e., application of vacuum while the solution is subjected to brief heating. For **2**, replacement of O_2 by either CO or PPh_3

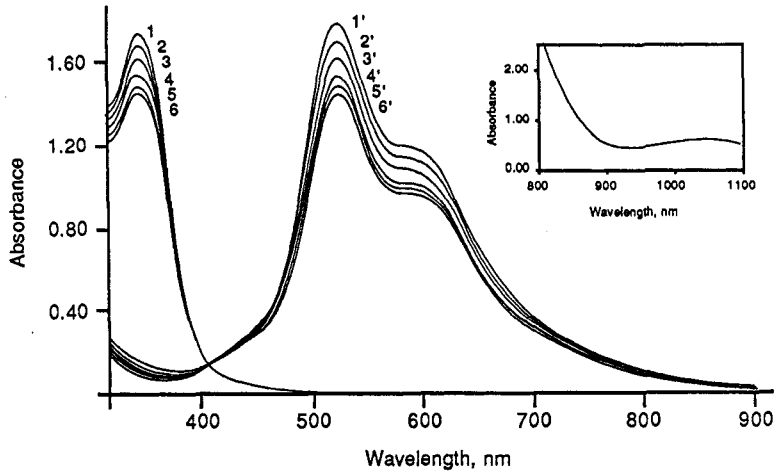

Fig. 4. Vacuum-cycling and associated UV-vis spectra to demonstrate reversible O_2 binding.

gives the adducts $[(TMPA)Cu(CO)]^+$ and $[(TMPA)Cu(PPh_3)]^+$, respectively. X-ray data obtained from crystals of $[\{(TMPA)Cu\}_2(O_2)][PF_6]_2 \cdot 5Et_2O$ (**2**·5Et_2O) at -90 °C revealed a *trans*-μ-1,2-(O_2^{2-})-dicopper(II) coordination. The Cu(II) ions are pentacoordinate with distorted trigonal-bipyramidal geometry, the peroxo oxygen atoms occupying the axial positions. The Cu-Cu distance is 4.359 Å and the O-O bond length is 1.432 Å. Resonance Raman studies showed an intraperoxide stretch (832 cm^{-1}) and a Cu-O stretch (561 cm^{-1}) (ref. 8). Complex **2** also exhibits silent EPR and nearly normal ^1H NMR spectra.

Magnetic susceptibility measurements performed on **2** indicated that $-2J > 600$ cm^{-1}, based on $\mathbf{H} = 2J\mathbf{S_1}\cdot\mathbf{S_2}$. These results suggest that a single bridging O_2^{2-} ligand can mediate strong magnetic coupling between two copper(II) ions. It is worthwhile to mention that although **2** is a functional model for hemocyanin, it lacks the precise spectroscopic and structural signatures of the active site of oxyhemocyanin, wherein $\eta^2{:}\eta^2$ O_2^{2-} to dicopper(II) binding has been determined from a recent X-ray crystal structure. Nevertheless, important insights into O_2 reactivity with Cu(I) species have been obtained from $[(TMPA)Cu(RCN)]^+$, especially from studies of the kinetics and thermodynamics of O_2 binding *(vide infra)*.

Fast Kinetic Study of $[(TMPA)Cu(RCN)]^+$

A detailed kinetic study of the oxygenation reaction of $[(TMPA)Cu(RCN)]^+$ was carried out using a variable temperature (-90 °C to room temperature) multiwavelength (359-776 nm) stopped-flow instrument (ref. 9). Complete data analysis provides the reaction mechanism as shown in Fig. 3. At low temperature, one molecule of complex **1** first reacts in a reversible fashion with O_2 to form a CuO_2 1:1 adduct $[(TMPA)Cu(O_2)]^+$ (**4**) intermediate, which then further reacts with another molecule of **1** to form the final Cu_2O_2 2:1 adduct $[\{(TMPA)Cu\}_2(O_2)]^{2+}$ (**2**). Complete data analysis also provides spectroscopic characterizations for the CuO_2 1:1 adduct **4**, (λ_{max} = 410 nm, ε = 4000 M^{-1}cm^{-1}), and for the final Cu_2O_2 2:1 adduct **2**, (λ_{max} = 525 nm, ε = 15000 M^{-1}cm^{-1}). The latter agrees very well with UV-vis spectra recorded for **2** under the "synthetic" conditions *(vide supra)*. Kinetic and thermodynamic parameters for each individual step have been solved as well. At -90 °C, $k_1 = 2 \times 10^4$ (M^{-1}s^{-1}), $K_1 = 1.9 \times 10^3$ (M^{-1}); $k_{on} = (k_1k_2/k_{-1}) = 6 \times 10^7$ (M^{-2}s^{-1}) and $K_1K_2 = 4 \times 10^{11}$ (M^{-2}). It is interesting to compare the kinetic and thermodynamic parameters for the formation of the CuO_2 1:1 adduct **4** with proteins and other synthetic model systems which form O_2-complexes with the same stoichiometry. From Table 2, it is apparent that the rate of $[(TMPA)Cu(O_2)]^+$ (**4**) formation at room temperature ($k_1 \sim 10^7$ M^{-1}s^{-1}) is comparable with

TABLE 2. Kinetic and Equilibrium Constants for O_2 Binding at Room Temperature.

System	k_1 (O_2) (M^{-1}s^{-1})	K_1 (M^{-1})
Mb (sperm whale myoglobin)	2.3×10^7	9.7×10^5
Hb (hemoglobin), R State	3×10^7	2×10^6
Hb (hemoglobin), T State	7×10^6	5×10^3
Picket-fence, R State	4.3×10^8	1.5×10^5
Picket-fence, T State	1.1×10^8	2.4×10^3
Pocket-picket, R State	2.2×10^6	2.4×10^5
Chelated heme		
short tail	4.9×10^7	3.1×10^5
medium tail	2.2×10^7	9.6×10^5
long tail	2.9×10^7	1.2×10^6
Strapped heme		
tight strap	3×10^5	
loose strap	1.7×10^6	6.8×10^3
Cu(I) mononuclear complexes §	6×10^5-9×10^7	0.28-0.60
Cytochrome *c* oxidase	3.5×10^8	7.0×10^3
LCo^{2+} (L = C-meso-Me$_6$[14]aneN4)		
LCo^{2+}	5.0×10^6	301
$(Cl)LCo^{2+}$	1.8×10^6	560
$[Co(l\text{-histidinato})_2]^{2+}$	3.5×10^3	
Hemerythrin (Hr) (octamer P.g.) *	1.2×10^7	2.8×10^5
Hemocyanin (Hc) (monomer P.i.) *	5.7×10^7	5.7×10^5
Hemocyanin (Hc) (hexamer P.i.) *	3.1×10^5	5.2×10^5
$[Cu_2XYL\text{-}H]^{2+}$ *	4570 (20 °C)	6
$[Cu_2XYL\text{-}O]^+$ *	$> 10^6$ (-80 °C)	35 (25 °C)

§ This work * M_2O_2 is formed during the oxygenation reaction

those for iron proteins Hb/Mb, porphyrin-iron model complexes, and for cytochrome *c* oxidase (generally in the range 10^5-10^8 M^{-1}s^{-1}), although the equilibrium constant for CuO_2 formation ($K_1 = 0.3$ M^{-1}) is dramatically smaller than those for the aforementioned proteins and model complexes (in the range of 10^3-10^5 M^{-1}). The reason for the less stable 1:1 O_2 adduct of the complex $[(TMPA)Cu(RCN)]^+$ is the highly unfavorable negative reaction entropy $\Delta S°$, which we think derives from the lack of optimized electronic

and steric conditions in our copper model system; such conditions, of course, are typically found in the multisubunit organization of proteins. Comparing the rate constant k_{on} -- representing the overall formation of the final Cu_2O_2 adduct -- with Co(II) systems, we find gross similarity for the peroxo-dicobalt(III) Co_2O_2 adducts analogously derived from mononuclear LCo(II) (L = N4-macrocycle) complexes, (i.e., $k_{on} = 10^8$-10^9 $M^{-2}s^{-1}$). These Co_2O_2 complexes also exhibit large negative $\Delta S°$ values, but still have considerable room temperature stabilities. The latter are derived from much larger negative $\Delta H°$ values for K_1K_2.

C *c*O: THE ENZYME ACTIVE SITE AND MODELS FOR O_2 REACTIVITY

Cytochrome *c* oxidase (C*c*O) is a terminal respiratory protein which catalyzes the four-electron four-proton reduction of O_2 to water (ref 10). The reduction of O_2 occurs at a dinuclear metal site which consists of a heme a_3 strongly spin coupled ($-J > 50$ cm^{-1}) with a Cu_B center in the resting oxidized state (Fig. 5). The nature and the identity of the bridging ligand which mediates the antiferromagnetic coupling betweeen the metal centers is not yet clear. However, μ-chloro, μ-sulfido and μ-oxo groups have been proposed as possible bridging ligands in the oxidized dinuclear site and the distance between the Fe and Cu centers is thought to be less than 5 Å. A second heme (heme *a*, low spin iron(III)) and a second copper (Cu_A) are also known to play a role in the O_2 reduction process by mediating the transfer of electrons from the electron carrier cytochrome *c* to the dinuclear site. This electron transfer process is coupled to proton translocation across the cell membrane. The electrochemical potential gradient generated by this proton pumping process is ultimately used in the synthesis of ATP.

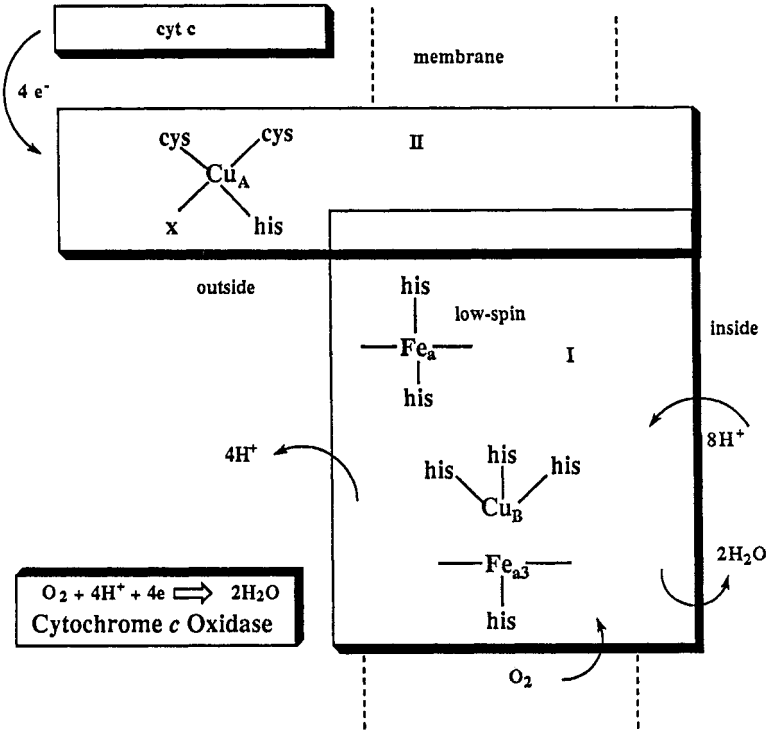

Fig. 5. A representation of C*c*O function.

As indicated in Fig. 6, the resting oxidized Fe(III)...Cu(II) state is converted to an active reduced Fe(II)...Cu(I) state by a two step 2-e^- process. Kinetic and spectroscopic evidence point to Cu_B as the initial binding site for O_2, thus implicating the importance of Cu(I)-O_2 reactivity in the O_2 reduction process of C*c*O (ref 10d). The bound O_2 is rapidly converted to a peroxo-iron(III) state, which after protonation and a third electron transfer step induces cleavage of the O-O bond to generate a ferryl Fe^{IV}-oxo species. The resting oxidized state is regenerated after the fourth electron transfer and protonation.

Although the reactivity of O_2 with both Fe(II) porphyrins and Cu(I) complexes have separately been studied in detail, few attempts have been made to characterize the products associated with the reaction of O_2 with both (ref. 11). We have synthesized a dinuclear oxo-bridged Fe-Cu complex which exhibits a

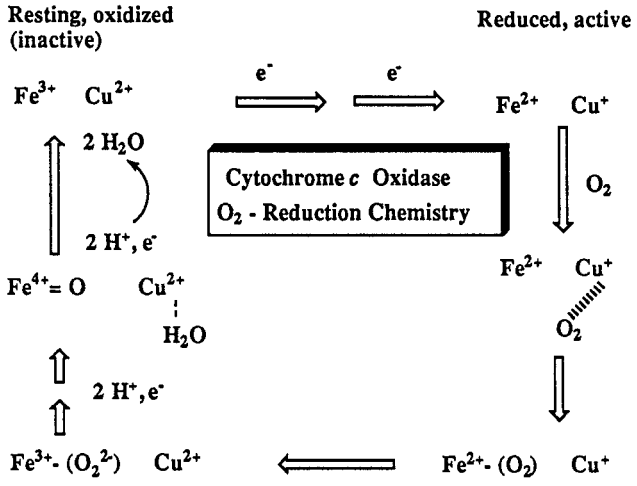

Fig. 6. A mechanism indicating generation and consumption of putative intermediates involved in CcO.

strong antiferromagnetic coupling between the Fe and Cu centers, by reacting an iron(II) porphyrin and **1** in the presence of O_2. TMPA was found to be an appropriate ligand for such studies since a recent report indicates a four N-ligand coordination for Cu_B in cytochrome ba_3 from *Thermus thermophilus* (ref 10a). Several model compounds comprising bridging oxo, imidazolato and sulfur containing ligands have been synthesized and characterized (ref. 11). By having either an intermediate spin iron(III) or a weakly coupled iron-copper dinuclear center, however, they don't precisely represent the resting state in CcO.

Synthesis and characterization of oxo/hydroxo bridged iron-copper dinuclear complexes

When an equimolar mixture of (F_8-TPP)Fe(II)pip$_2$ (pip = piperidine) (**5**) (Fig. 7) and [(TMPA)Cu]$^+$ (**1**) were allowed to react at -80° C in CH_2Cl_2 in the presence of O_2 and warmed to 0° C, a purple-red solid could be isolated by precipitation with heptane (yield > 80%). A microcrystalline solid formulated as [(F_8-TPP)Fe-(O^{2-})-Cu(TMPA)]$^+$ (**6**) was isolated by dissolution of the crude product in acetonitrile and reprecipitation by slow addition of diethylether in an overall isolated yield of 50 %. Interestingly, the reaction of equimolar amounts of [Cu(TMPA)(CH_3CN)][ClO_4]$_2$ (**7**), (F_8-TPP)Fe-OH (**8**), and Et_3N in CH_3CN under argon generated a red micro-crystalline product, in 80% yield, identified as **6** on the basis

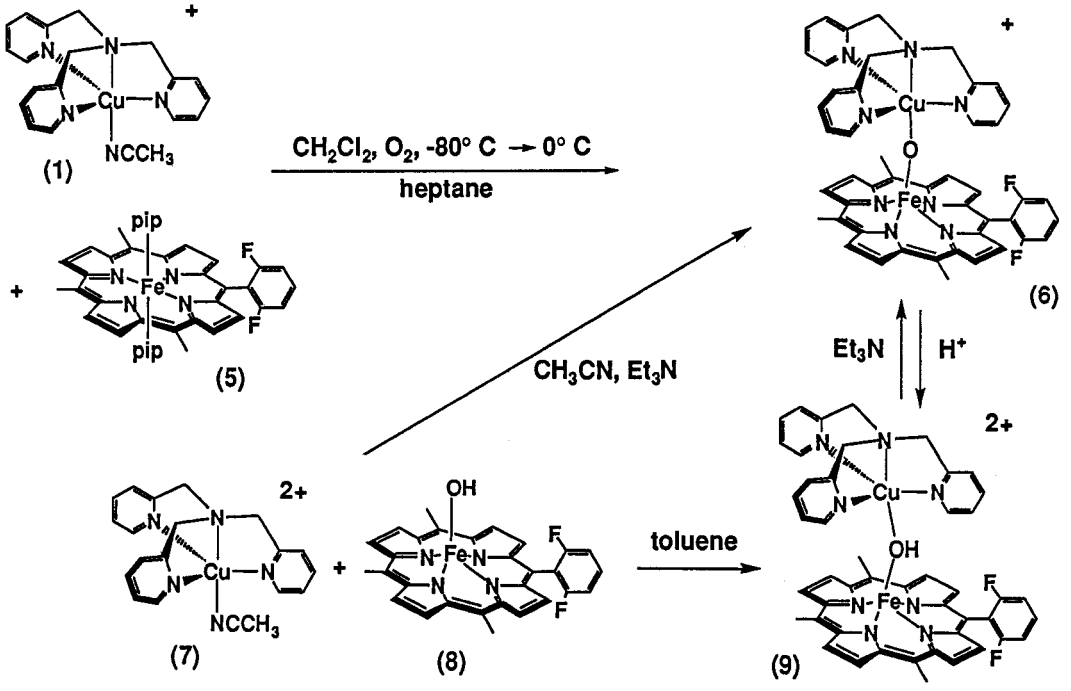

Fig. 7. Synthesis and interconversion of μ-oxo and μ-hydroxo porphyrin-iron-copper complexes.

of its identical UV-vis and ^1H NMR spectra. Subsequent recrystallization from CH_2Cl_2/heptane yielded single crystals which gave comparable elemental analysis to **6** generated from O_2. An X-ray structure was obtained of a crystal generated by this method. The structure reveals a linear Fe(III)-oxo-Cu(II) coordination (Fe-O-Cu = 178.2 (4)°), and Fe-O and Cu-O bond distances of 1.740 Å (5) and 1.856 Å (5) respectively. The bond distances associated with the coordination of iron are similar to those reported for μ-oxo bridged iron-porphyrin dimers. The coordination environment around Cu is distorted square-pyramidal, not the more usual trigonal bipyramidal geometry; the three pyridine rings appear to sit in between the four difluorophenyl groups of the porphyrin, thereby leaving one 'slot' free.

Mössbauer spectroscopic measurements of **6** indicate a high-spin iron(III) porphyrin (zero-field spectrum; $\delta = 0.47 \pm 0.01$ mm/s; $\Delta E_Q = 1.26 \pm 0.02$ mm/s) strongly coupled to Cu(II) to give a S = 2 spin system. Variable temperature magnetization studies also show an excellent fit for an S = 2 model, which indicates that the exchange coupling is large and antiferromagnetic. A J value of -87 cm^{-1} was estimated based on $H = 2J\ S_1 \cdot S_2$ (to be published). A magnetic moment of 5.1 ± 0.1 B.M. was obtained both in solid state and solution (Evans method) also in agreement with a coupled S = 2 model. The pyrrole proton NMR signal is observed at 65 ppm (in CD_2Cl_2 or CD_3CN) and is shifted upfield relative to axially symmetric five-coordinate high-spin iron(III) tetraphenylporphyrin (TPP) complexes, which generally show a pyrrole NMR signal at 80 ppm (ref 12). An upfield shift is expected for an antiferromagnetically coupled system since high-spin iron(II) (S = 2) TPP complexes exhibit a pyrrole proton NMR signal in the 30-61 ppm region (ref 13). The UV-vis spectrum of **6** shows a Soret band at 434 nm and is shifted relative to other high-spin iron(III) TPP complexes, which are generally observed in the 400-415 nm region (ref 12). The red shift of the Soret band is surprising since μ-oxo bridged iron-porphyrin dimers do not show a similar trend, indicating that the copper-TMPA moiety dramatically alters the electronic properties of the iron-oxo moiety. The IR spectrum of **6** (solid, nujol) showed a new band at 856 cm^{-1}, which is in the general region where the Fe-O-Fe antisymmetric stretch has been reported for most oxo-bridged iron complexes (ref. 14). Use of $^{18}O_2$ gas in the synthesis resulted in lowering of the intensity of this band with corresponding changes in the 780-790 cm^{-1} region. A firm assignment cannot be made at this time, however, due to the overlap of strong porphyrin and TMPA ligand absorptions in this region. The antisymmetric vibration of [(F_8-TPP)Fe-O-Fe(F_8-TPP)] occurs at 867 cm^{-1}.

Protonation of **6** by addition of an equivalent of triflic acid in dichloromethane produced a new species formulated as [(F_8-TPP)Fe-(OH)-Cu(TMPA)]$^{2+}$ (**9**). The perchlorate analog of **9** could also be isolated by reacting an equimolar mixture of [(TMPA)Cu(CH_3CN)][ClO_4]$_2$ (**7**) and [(F_8-TPP)Fe-OH] (**8**) in toluene or dichloromethane. This species shows a pyrrole proton NMR signal at 69 ppm in CD_2Cl_2 and a solution magnetic moment of 5.5 ± 0.1 B.M. (Evans method), which points to a weakening of coupling between the Fe and Cu centers as a result of protonation. As expected, deprotonation of **9** by addition of an equivalent of Et_3N regenerates complex **6** (Fig. 7).

CONCLUSION

Our group has investigated bioinorganic Cu-O_2 chemistry since the early 1980's. One of our most significant findings has been the synthesis and characterization of the mononuclear copper (I) complex [(TMPA)Cu(RCN)]$^+$ (**1**), which binds O_2 reversibly at -80 °C in EtCN or CH_2Cl_2 to give the structurally characterized 2:1 (Cu:O_2) *trans*-μ-1, 2-peroxo adduct [{(TMPA)Cu}$_2$(O_2)]$^{2+}$ (**2**), the prototypical functional model complex for the metalloprotein hemocyanin. From associated stopped-flow kinetic and UV-vis spectral studies, it was deduced that the 1:1 adduct [(TMPA)Cu(O_2)]$^+$ (**4**), a putative cupric superoxide species, forms initially and then reacts with another equivalent of **1** to give the 2:1 adduct **2**. The rate constant k_1 for the formation of **4** from **1** and O_2 was determined to be 2 x 10^4 M^{-1} s^{-1} at -90 °C, which extrapolates to *ca.* 10^7 M^{-1} s^{-1} at -25 °C, the same order of magnitude as the O_2 transporting proteins hemoglobin and myoglobin, as well as model heme complexes. It also compares with k_1 for the 2:1 (M:O_2) proteins hemerythrin (M = Fe) and hemocyanin.

Cytochrome *c* oxidase (C*c*O) binds O_2 at near diffusion-control rates (k_1 = 3.5 x 10^8 M^{-1} s^{-1} at -25 °C), but detailed knowledge of M:O_2 (M = Fe, Cu) interactions, not to mention the possible subsequent intermediates, remains elusive. Our original model approach employs a ferrous-porphyrin, (F_8-TPP)Fepip$_2$ (**5**), and our reactive cuprous complex **1**, in the presence of O_2; the unusual μ-oxo bridged [(F_8-TPP)Fe-O-Cu(TMPA)]$^+$ (**6**) complex is generated in *ca.* 80% yield. A full description of its structural, spectral, and magnetic properties is in preparation; also, **6** can be readily protonated to yield the putative μ-hydroxo analogue **9**. Complexes **6** and **9** serve as models for possible intermediates generated during the O_2 reduction cycle of C*c*O, and experiments to determine their mechanism(s) of formation are in progress.

REFERENCES

(1) K.D. Karlin and Z. Tyeklár, Ed., Bioinorganic Chemistry of Copper, Chapman & Hall, New York (1993).
(2) (a) Z. Tyeklár and K.D. Karlin, Acc. Chem. Res. 22, 241-248 (1989). (b) K.D. Karlin, Z. Tyeklár, and A.D. Zuberbühler, Bioinorganic Catalysis, p. 261-315, Marcel Dekker, New York (1992). (c) Z. Tyeklár, and K.D. Karlin, Bioinorganic Chemistry of Copper, p. 277-291, Chapman & Hall, New York (1993).
(3) N. Kitajima, Adv. Inorg. Chem. 39, 1-77 (1992).
(4) M.S. Nasir, B.I. Cohen and K.D. Karlin, J. Am. Chem. Soc. 14, 2482-2494 (1992).
(5) (a) B. Hazes, K.A. Magnus, C. Bonaventura, J. Bonaventura, Z. Dauter, K.H. Kalk and W.G.J. Hol, Protein Science 2, 597-619 (1993). (b) K.A. Magnus, H. Ton-That and J.E. Carpenter, Bioinorganic Chemistry of Copper, p 143-150, Chapman & Hall, New York (1993).
(6) E.I. Solomon, M.J. Baldwin and M.D. Lowery, Chem. Rev. 92, 521-542 (1992).
(7) (a) Z. Tyeklár, R. R. Jacobson, N. Wei, N. Narasimha Murthy, J. Zubieta and K. D. Karlin, J. Am. Chem. Soc. 115, 2677-2689 (1993).
(8) M.J. Baldwin, P.K. Ross, J.E. Pate, Z. Tyeklár, K.D. Karlin, and E.I. Solomon, J. Am. Chem. Soc. 113, 8671-8679 (1991).
(9) (a) K.D. Karlin, N. Wei, B. Jung, S. Kaderli and A.D. Zuberbühler, J. Am. Chem. Soc. 113, 5868-5870 (1991). (b) K.D. Karlin et. al. Submitted.
(10) (a) J.A. Fee, W.E. Antholine, C. Fan, R.J. Gurbiel, K. Surerus, M. Werst and B.M. Hoffman, Bioinorganic Chemistry of Copper, p 485-500, Chapman & Hall, New York (1993). (b) G.T. Babcock and M. Wikström, Nature 356, 301-309 (1992) and references cited therein. (c) R.A. Scott, Annu. Rev. Biophys. Chem. 18, 137-158 (1989). (d) C. Varotsis, Y. Zhang, E. H. Appelman and G. T. Babcock, Proc. Natl. Acad. Sci. USA 90, 237-241 (1993).
(11) A. Nanthakumar, M.S. Nasir, N. Ravi, B.H. Huynh and K.D. Karlin, J. Am. Chem. Soc. 114, 6564-6566 (1992) and references cited therein. (b) A. Nanthakumar et. al. submitted.
(12) M.A. Phillippi and H.M. Goff, J. Am. Chem. Soc. 104, 6026-6034 (1982).
(13) A. Shirazi and H.M. Goff, J. Am. Chem. Soc. 104, 6318-6322 (1982).
(14) D.M. Kurtz, Chem. Rev. 90, 585-606 (1990).